

**Title:** MEMS-actuated Metasurface Alvarez Lens

**Author List:**

Zheyi Han<sup>1</sup>, Shane Colburn<sup>1</sup>, Arka Majumdar<sup>1,2</sup>, & Karl Böhringer<sup>1,3,4,\*</sup>

<sup>1</sup>Department of Electrical and Computer Engineering, University of Washington, Seattle, Washington 98195, USA.

<sup>2</sup>Department of Physics, University of Washington, Seattle, Washington 98195, USA.

<sup>3</sup>Department of Bioengineering, University of Washington, Seattle, Washington 98195, USA.

<sup>4</sup>Institute for Nano-engineered Systems, University of Washington, Washington 98195, USA.

\*Correspondence to: [karlb@uw.edu](mailto:karlb@uw.edu)

**Abstract:**

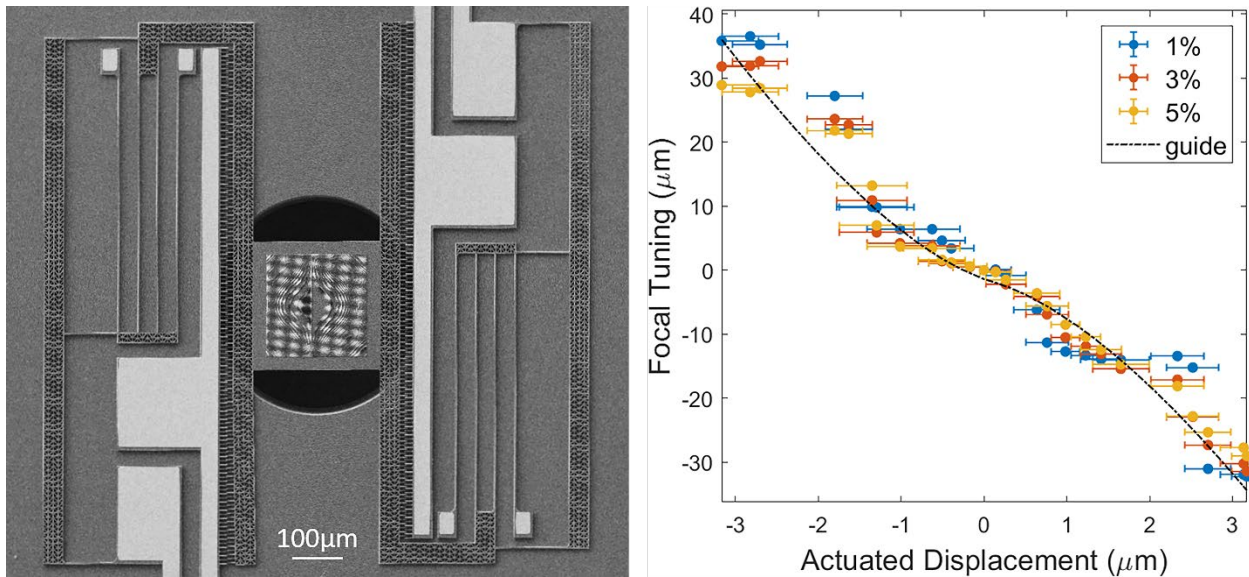
Miniature lenses with tunable focus are essential components for many modern applications involving compact optical systems. While several tunable lenses have been reported with various tuning mechanisms, they often still face challenges in power consumption, tuning speed, fabrication cost, or production scalability. In this work, we have adapted the mechanism of an Alvarez lens – a varifocal composite lens in which lateral shifts of two optical elements with cubic phase surfaces give rise to a change in optical power – to construct a miniature, MEMS-actuated metasurface Alvarez lens. The implementation based on electrostatic microelectromechanical systems (MEMS) generates fast and controllable actuation with low power consumption. The utilization of metasurfaces, ultrathin and subwavelength-patterned diffractive optics, as the optical elements greatly reduces the device volume compared to systems using conventional freeform lenses. The entire MEMS Alvarez metalens is fully compatible with modern semiconductor fabrication technologies, granting it the potential to be mass-produced at a low unit cost. In the

reported prototype, a total uniaxial displacement of  $6.3\ \mu\text{m}$  is achieved in the Alvarez metalens with direct-current (DC) voltage application up to 20 V, modulating the focal position within a total tuning range of  $68\ \mu\text{m}$ , producing more than an order of magnitude change in focal length and 1460 diopters change in optical power. The MEMS Alvarez metalens has a robust design that can potentially generate much larger tuning range without substantially increasing device volume or energy consumption, making it desirable for a wide range of imaging and display applications.

**Keywords:**

Microelectromechanical Systems, Metasurface, Varifocal Lens, Alvarez Lens, Diffractive Optics, Tunable Metasurface

**TOC Graphic:**



## **Introduction:**

Miniature focus-tunable optical elements are crucial for various applications, where the size and weight of the optics are highly constrained. For example, optical components used in mobile applications, entertainment, robotics, surveillance, aerospace, and biomedical systems often need to be tunable within a large focal length range while maintaining reliability and cost-effectiveness [1, 2]. Conventional tunable imaging systems often have either bulky optical elements that are challenging to mass-produce, such as liquid tunable lenses [3], or tuning mechanisms that require a large volume for actuation of elements, such as physically translating the lens along the optical axis [4]. A miniaturized optical element together with an efficient tuning mechanism is essential for designing a compact tunable lens system.

Metasurface optics is a novel replacement for bulky freeform optical elements with greatly reduced volume and high compatibility with modern microfabrication processes. These elements are two-dimensional, quasi-periodic arrays of sub-wavelength scatterers arranged to arbitrarily control the phase, amplitude, and polarization of electromagnetic waves by imparting an abrupt, spatially varying phase profile on the incident light [5]. With metasurfaces, complex and bulky geometric lens curvatures can be converted into a discretized spatial phase profile on a flat, wavelength-scale thick surface [6-10]. The corresponding fabrication process can employ mature semiconductor nanofabrication technologies that are readily scalable for mass production.

There have been multiple works attempting to modulate the optical power of metasurfaces with various mechanisms. Ee et al. designed and fabricated a mechanically reconfigurable metasurface on a stretchable membrane for the visible frequency range, with the deformation induced by four clamps individually mounted on translation stages [11]. The design by She et al. combined metasurface optics with a dielectric elastomer actuator to create an electrically tunable

focal length by electrostatically compressing the elastomer in the direction of its thickness leading to a lateral expansion in both the elastomer and the carried metasurface; however, due to the limitations in the elastomer viscoelasticity, charge transfer, and dissipation time in electrodes, the response time of their design is capped at 33 ms [12]. Roy et al. designed a microscale tunable mirror by placing a reflective metasurface lens on top of a 2D electrically actuated scanner platform [13]. The angular rotation of the mirror plate scans the focal position of the metasurface lens by several degrees in a three-dimensional space. The manual assembly required to integrate the individual MEMS mirror and the external MEMS platform inevitably increases the overall fabrication time, rendering the device less desirable for mass production. Arbabi et al. fabricated and demonstrated a tunable metasurface doublet lens realized by vertical MEMS actuation. Their system comprised both converging and diverging metasurface lenses assembled on top of each other, giving a tunable focal distance controlled by the separation electrostatically varied between the two lenses [14]. While this method can provide a change in focal length inversely proportional to the vertical displacement, the fabrication entails an initial separation between lenses to reserve space for the designed actuation, which limits the overall tuning range if a thin device is desired. Additionally, the parallel plate actuator in their design can only increase the focal length from the initial value by decreasing the optics separation rather than tuning in both directions.

A separate approach for creating a miniature lens system with tunable optical power is based on Alvarez lenses [15-17]. A typical Alvarez lens contains a pair of optical elements with complementary cubic surface profiles. Optical power modulation is achieved by the relative lateral displacement between the two optical elements in the direction perpendicular to the optical axis. In this way, the focal length change is inversely proportional to the lateral displacement, and the focal length can be tuned in both directions. Previously some researchers integrated a pair of

miniature, freeform optics with cubic surface profiles with a MEMS actuator to electrostatically displace the optical elements laterally for focus tuning within a compact package [18, 19]. In these works, however, the lens elements and the MEMS structure were manufactured separately and then manually assembled, requiring additional time and cost. Moreover, the conventional refractive optics used in these Alvarez systems require complex 3D geometries to produce the desired cubic surfaces for optimal performance and mounting for assembly requirements. This often requires complicated fabrication and at the same time can be a substantial obstacle to further miniaturization.

A possible solution to create a miniature, focus-tunable optical system compatible with large-scale microfabrication is to convert the 3D Alvarez optical elements into a pair of 2D metasurface optics with complementary cubic surface profiles, which can be integrated with a micro-scale MEMS-actuated structure to introduce lateral displacement for optical modulation. Metasurface Alvarez lenses have shown great potential for substantial focal length control with small relative lateral shifts. Recent works have demonstrated an Alvarez metalens inducing 2.5 mm focal tuning range in visible wavelengths over a 100  $\mu\text{m}$  actuation range with a 150  $\mu\text{m}$  wide square aperture [1] and another inducing a 6.62 cm focal tuning range in the infrared (IR) spectrum over a 2.75 mm actuation range with a 1 cm wide square aperture [2]. Currently, however, the displacement has been performed using optomechanical stages actuated manually, while a compact and electrically controllable solution has not been demonstrated.

In this work, we present a silicon nitride metasurface-based Alvarez lens actuated by an electrostatic MEMS platform, capable of producing focal length modulation 10 times larger than the actuated displacement. The metasurfaces are fabricated with high-throughput stepper lithography and the entire structure is fully compatible with well-developed semiconductor

nanofabrication technologies, providing high reliability, low cost, and the potential for production scalability.

## **Results:**

### Design of MEMS-actuated Metasurface Platform

A miniature MEMS electrostatic actuator has been implemented to laterally displace one of the complementary Alvarez metasurface optics relative to the other with high precision and speed. Since a conventional Alvarez lens requires symmetric actuation of both phase masks, in our configuration, where only one of the Alvarez plate pairs is actuated to enhance robustness in prototype fabrication and operation, a lateral shift of the optical axis, albeit a small one, is also induced during focal length modulation. The actuator design for the moving metasurface is based on conventional linear comb drives [20] and exact constraint folded flexures [21] to introduce the electrostatic driving force and to generate the mechanical restoring force, respectively.

Electrostatic comb drives can induce efficient, controllable displacement at low power; hence, they are often popular candidates for microscale devices designed for sensing and micropositioning. A typical design of a comb drive actuator consists of two comb structures with interdigitated fingers, of which one is fixed while the other is connected to a compliant suspension. A voltage applied across the two comb structures will lead to a deflection of the movable comb drawn by the electrostatic forces created in the capacitors between the fingers with different potentials. Since the electrostatic forces are created by capacitive interactions without any physical contact between the two combs, there is no DC current flowing in the device, realizing low power actuation. The design of using an array of small fingers instead of one single large parallel plate capacitor significantly increases the area for capacitive interaction and hence the resultant electrostatic force with a given applied voltage. Moreover, the linear comb design allows

controlled motion over a larger displacement range compared to the parallel plate capacitor. The substrate and the mobile comb are usually grounded to prevent the development of electrostatic pull-down forces acting on structures in suspension, and only the stationary comb is at a non-zero potential to generate an electrostatic driving force between the combs.

With the assumption that the fringing field effect is negligible, the total capacitance between the interdigitated fingers in each comb drive can be estimated as

$$C_{total} = 2N \frac{\epsilon l h}{d}, \quad (1)$$

where  $N$  is the number of finger pairs,  $\epsilon$  is the permittivity of the medium between the fingers which have interdigitating length  $l$ , height  $h$ , and separation  $d$ . With a voltage  $V$  applied across the comb drive, the corresponding electrostatic force becomes

$$F_{el}(V) = \frac{dW(V)}{dl} = \frac{d}{dl} \left( \frac{1}{2} C_{total} V^2 \right) = \frac{N \epsilon h V^2}{d}. \quad (2)$$

If the movable comb, carrying the metasurface platform, is connected to some mechanical flexure with a spring constant  $k$ , then at equilibrium, the lateral displacement of the movable comb is

$$x(V) = \frac{F_{el}(V)}{k} = \frac{N \epsilon h V^2}{k d}. \quad (3)$$

Note that the actuated displacement is linearly proportional to the electrostatic force, making a comb drive a better choice for large displacements than parallel plate capacitors. Since the physical dimensions and material properties do not change after fabrication, with proper device calibration, the exact actuated displacement can be predicted by Eq. (3) at any given actuation voltage. Such controllability makes comb-drive actuators very attractive structures for applications involving micropositioning.

For unidirectional actuation, we need a suspension platform, which is compliant along the direction of the desired movement but stiff in orthogonal directions. To enable that, we employ

the mechanical structures of the actuators from the exact constraint folded flexure [21]. By constraining the displacement of the intermediate body with a 1:2 lever, we can reduce the development of extensional axial forces, preventing motion sideways or rotation when a lateral displacement is actuated. The mechanical stiffness of the actuator in the direction of lateral displacement can be estimated with the lateral spring constant of the folded flexure

$$k_x = \frac{2Ehb^3}{L^3}, \quad (4)$$

with  $E$  being Young's modulus of single-crystal silicon,  $h$  the device layer thickness (also the spring beam and finger height),  $b$  the width of spring beams, and  $L$  the length of individual beams. For all our actuators,  $L = 500 \mu\text{m}$ ;  $b = 4 \mu\text{m}$  and  $h = 5$  or  $6 \mu\text{m}$  are the design parameters. With  $E = 130 \text{ GPa}$  in the silicon-100 plane [22], an actuator will have a lateral stiffness of  $0.666 \text{ N/m}$  ( $0.799 \text{ N/m}$ ) for  $h$  of  $5 \mu\text{m}$  ( $6 \mu\text{m}$ ). The effect of the additional 1:2 lever is difficult to calculate analytically but is expected to slightly increase the value of stiffness.

Figure 1 shows the scanning electron microscope (SEM) and optical images of a fabricated MEMS actuator for carrying the mobile metasurface of the Alvarez pair, which is then aligned and bonded on top of the complementary metasurface fabricated on a stationary substrate. The microfabrication flow can be found in the Supporting Information. As shown in Figure 1a, the actuator design used here has two sets of comb drives and folded flexures on the opposite sides of the platform to double the actuation range under signals applied alternatively on both sides of the actuator and to prevent rotational displacement during the movement. Figure 1b shows a zoomed-in SEM image of a comb drive. The suspended left comb is attached to the central platform for displacement while the stationary right comb is anchored to the substrate. One of the silicon nitride Alvarez metasurfaces is carried by the central platform attached to the suspended combs of each set of comb drive while the other is fabricated on a stationary silicon substrate. Figure 1c shows

the details of one metasurface composed of a 2D array of cylindrical silicon nitride nanoposts, generating the desired phase profile for the Alvarez optics. Figure 1d and 1e show optical images of the two Alvarez metasurfaces with complementary surface profiles. The two chips carrying the metasurfaces are overlaid on top of each other in the bonded lens system.

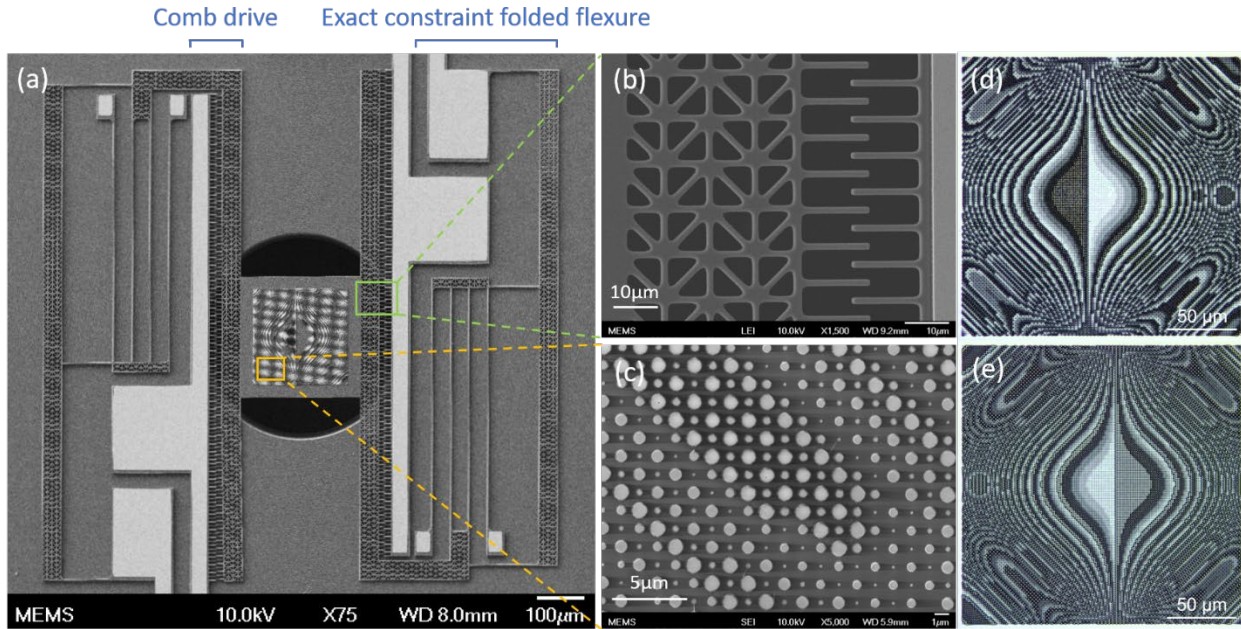


**Figure 1.** SEM image of (a) a MEMS-actuated platform carrying the movable metasurface in an Alvarez metalens, with (b) and (c) being the zoomed-in SEM images portraying the electrostatic comb drive and the metasurface nanoposts. (d, e) Optical images of the Alvarez metasurfaces with complementary cubic phase profiles that are overlaid on top of each other in the assembled Alvarez metalens and in summation impart a quadratic phase change on the incident light.

### MEMS-actuated Metasurface Singlet Lens

Prior to testing the metasurface Alvarez lens, we fabricated a separate structure with a singlet converging metasurface lens with a diameter of 200  $\mu\text{m}$  on the central platform of the MEMS actuator to aid motion tracking by examining the movement of the focal spot (Figure 2a). The metasurface design followed the usual procedure [23] which is outlined in the Supporting Information. The left and right sides of the platform were attached to two sets of comb drives respectively. The prototype actuator was fabricated with 2 comb drive sets per side (with 125

finger pairs in each) and a device layer thickness of 6  $\mu\text{m}$ . With the MEMS actuator chip mounted on a glass stage, a superluminescent diode (SLD) source of 1550 nm illuminated the metasurface lens from the back. The resulting focal spot was monitored by an IR camera in front as an indication of the lens location (the experimental setup is described in the Supporting Information). Since the focal spot was located approximately 200  $\mu\text{m}$  in front of the metasurface, for demonstration of the relative lateral position of the metasurface and the focal spot, Figure 2a is an image overlay of the device surface plane and the focal plane. A DC voltage increasing from 0 V to 18 V and then back to 0 V with a step size of 500 mV was applied to the right comb drive sets of the actuator to electrostatically pull the central platform. The increasing voltage pulled the metasurface and the focal spot towards the right. By turning down the voltage, the focal spot relaxed back to its neutral position equilibrated by the spring force in the flexures. Figure 2b plots both the displacement of the focal spot and the applied voltages as time elapses, showing a clear positive correlation between the actuated displacement and voltage. The IR camera resolution limits the pixels available for focal spot tracking, giving rise to the distinctive steps in the focal location analysis. The symmetric displacement during voltage ramp-up and ramp-down in Figure 2b shows the absence of hysteresis and the reversibility of the platform actuation. The linear fit of the focal displacement (averaged over all captured video frames at each applied voltage) as a function of the voltage-squared further confirms that the actuated displacement is quadratically dependent on the voltage applied (see Figure 2c). The stiffness of the platform actuator can be calculated from the slope in Figure 2c according to Eq. (3), giving a spring constant of 0.713 N/m for this electrostatic actuator, which is 11% smaller than the analytically calculated value presented earlier, giving a softer device than predicted, probably due to fabrication discrepancies resulting in thinner structures. While we observe a displacement of 3.1  $\mu\text{m}$  under a voltage application of

18 V, if a voltage is applied to the left rather than the right side of the actuator, the metasurface can be displaced in the opposite direction, doubling the range of physical motion.

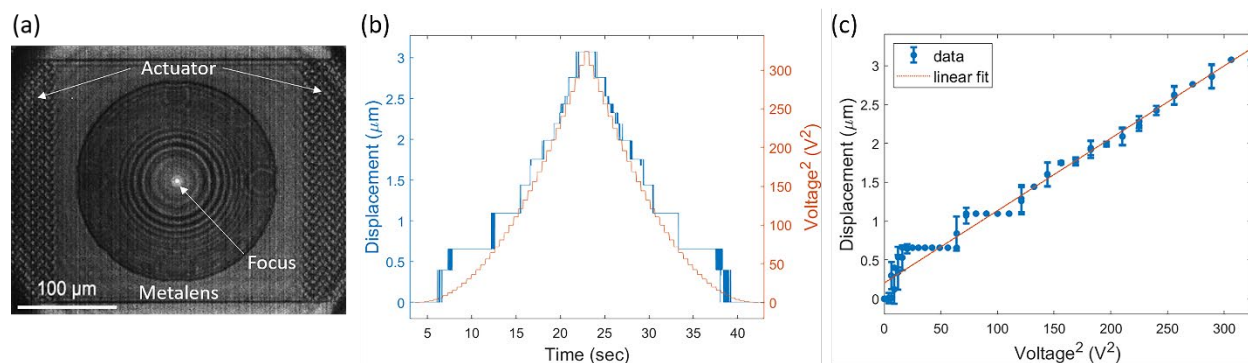


**Figure 2.** (a) Overlaid IR image showing both the device and focal planes of a singlet metalens on a MEMS-actuated platform. (b) Actuated focal displacement and applied voltage over time. The general trend of the actuated displacement follows the square of the applied voltages. (c) Average actuated displacement as a function of applied voltage-squared during both loading and unloading, showing a linear dependence. No hysteresis behavior is observed with voltage loading and unloading, verifying the reversibility of the actuation process.

### Design of Metasurface Alvarez Lens

With the electromechanical performance of the MEMS-actuated platform verified using a singlet metalens, we designed and fabricated the Alvarez lens device integrated with the MEMS platform for the IR spectrum consisting of two separate metasurfaces with an aperture of 200  $\mu\text{m}$ . When positioned with their surfaces parallel and aligned along the optical axis, the two Alvarez metasurfaces in conjunction form a singlet metalens imparting a quadratic phase profile onto the incident wavefront as shown in Figure 3a. The phase profiles of the regular and inverse metasurfaces of the Alvarez pair have the expressions [2]

$$\varphi_{reg}(x, y) = -\varphi_{inv}(x, y) = A \left( \frac{1}{3} x^3 + xy^2 \right). \quad (5)$$

A lateral displacement between the two metasurfaces modulates the optical power of the summed quadratic lens, where the constant  $A$  denotes the cubic phase strength chosen to produce a desirable

focal length tuning for a given aperture size and a designed displacement range. In a typical Alvarez lens, the phase masks are simultaneously translated in opposite directions by a displacement  $d$  (hence creating a total center-to-center offset of  $2d$  between the phase masks), producing a quadratic lens in summation with the expression

$$\varphi_{Alvarez}(x, y) = \varphi_{reg}(x + d, y) + \varphi_{inv}(x - d, y) = 2Ad(x^2 + y^2) + \frac{2}{3}Ad^3, \quad (6)$$

Neglecting the constant  $d^3$  term, we can relate the summed quadratic phase to that of a spherical singlet lens and express the focal length of the Alvarez lens as a function of the symmetric lateral displacement at a designed operating wavelength  $\lambda$  as

$$f(d) = \frac{\pi}{2\lambda Ad}. \quad (7)$$

A zero summed phase corresponding to a flat lens will be produced if the centers of the two Alvarez phase patterns are exactly aligned. For the specific Alvarez lens fabrication and experiments presented in this work, to accommodate data collection over our achievable actuation range with the current actuator designs, an initial offset of  $d = 10 \mu\text{m}$  has been introduced to the two metasurfaces respectively in opposite directions, hence giving a total of  $20 \mu\text{m}$  initial center-to-center lateral offset between the Alvarez phase masks as captured in Figure 3a.

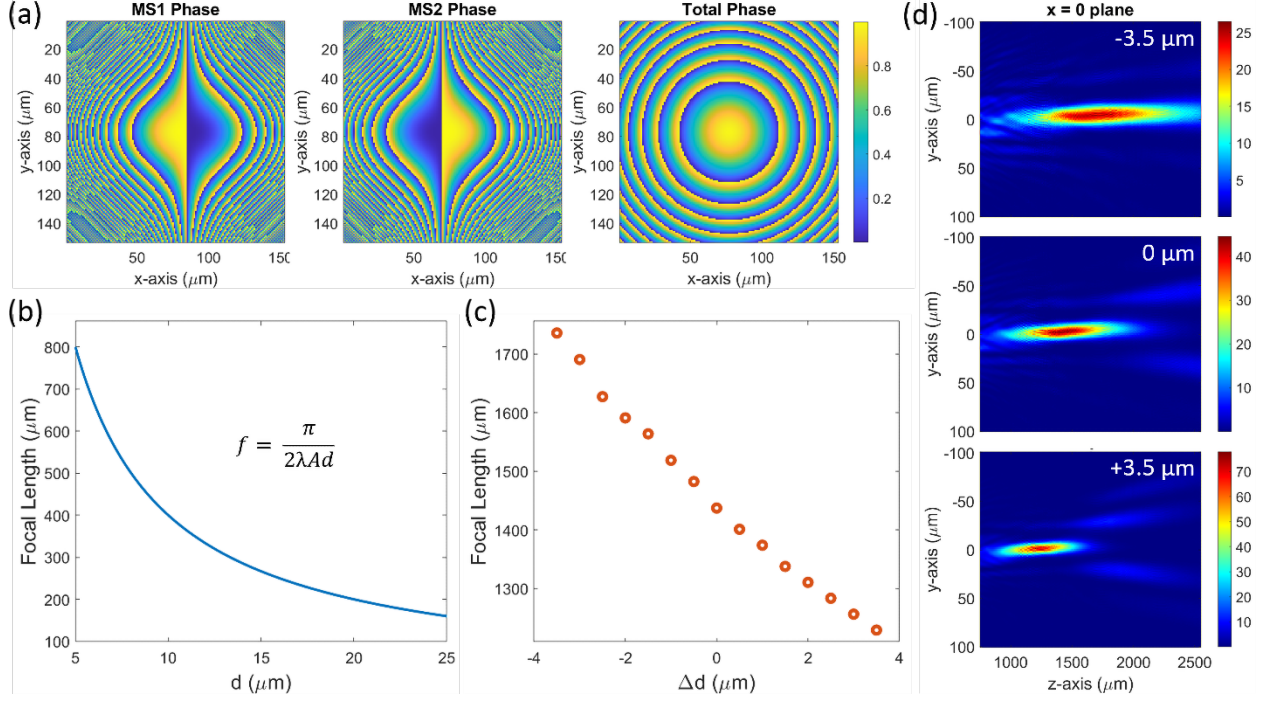


**Figure 3.** Metasurface Alvarez lens design and simulation. (a) Two  $200 \mu\text{m} \times 200 \mu\text{m}$  Alvarez metasurfaces with complementary cubic phase profiles and their summed quadratic phase when overlaid on top of each other. Phase values are normalized to  $2\pi$ . (b) Ideal Alvarez focal tuning behavior as a function of lateral symmetric displacement  $d$  (giving a total center-to-center offset of  $2d$ ) between the optical elements theorized with a negligible axial separation gap, an operating wavelength  $\lambda = 1550 \text{ nm}$  and a cubic parameter  $A = 2.5335 \times 10^{-14} \text{ m}^{-3}$  [2]. (c) Simulated focal tuning behavior when a small lateral displacement is introduced in addition to an initial center-to-center offset of  $20 \mu\text{m}$ , assuming a  $50 \mu\text{m}$  axial separation gap between the two metasurfaces from fabrication. The focal position is calculated from the weighted centroid of high-intensity regions. (d) Simulated change of focal location and profile when the two metasurfaces are laterally displaced at  $-3.5 \mu\text{m}$ ,  $0 \mu\text{m}$ , and  $+3.5 \mu\text{m}$ .

Figure 3b illustrates the ideal tuning behavior of a typical Alvarez lens assuming no axial separation exists between the two complementary phase masks, shows a nonlinear dependence of the focal position on the lateral offset. A larger center-to-center lateral offset between the Alvarez phase masks gives rise to a more rapidly varying phase profile, corresponding to a lens with a shorter focal length [1]. Figure 3c, instead of the ideal Alvarez behavior, shows the simulated behavior of the designed metasurface Alvarez lens under a more realistic situation in which an axial gap of  $50 \mu\text{m}$  is introduced between two metasurfaces from the bonding process and the

lateral displacement happens in small microscale steps as expected from the electrostatic MEMS actuator. Note that in our MEMS-actuated Alvarez metalens, in order to increase device robustness, only one metasurface phase mask is actuated relative to the other, instead of both phase masks being actuated simultaneously in opposite directions as in a conventional Alvarez lens. Hence the actuated displacement  $\Delta d$  presented in Figure 3c adds to the total center-to-center offset between the two metasurface phase plates, accompanied by a small translational shift of the optical axis during tuning. The 50  $\mu\text{m}$  axial separation gives rise to diffraction in the space between two metasurfaces, leading to distortion and shifting of the focal spot along the optical axis, as illustrated in Figure 3d. Specifically, the separation between two metasurfaces deviates the summed effects of the Alvarez elements from a simple phase addition. Instead of focusing onto a single point as expected by a singlet lens, the light incident on the Alvarez stack creates multiple closely spaced intensity maxima, forming an elongated and aberrated intensity cluster along the optical axis (Figure 3d). We denote the focal length as the centroid of the high-intensity clusters and plot the location of the centroid as a function of the displacement in Figure 3c. The simulation reveals close-to-linear tuning of the focal length with sub-micron displacement steps.

#### MEMS-actuated Metasurface Alvarez Lens

A full metasurface Alvarez lens was fabricated with the process flow described in the Supporting Information, with one Alvarez metasurface on the actuator membrane while the other on a stationary surface. The electrostatic actuator used for the Alvarez lens had 2 comb drive sets per actuation side with a device layer thickness of 5  $\mu\text{m}$ . The focal tuning of the metasurface Alvarez lens was measured with the Alvarez chip mounted on a translation stage and illuminated with a 1550 nm SLD source. A voltage between 0 and 20 V was applied to the comb drive to actuate the central metasurface platform, changing the lateral offset between two Alvarez

metasurfaces. At any point in time, we actuated the comb drives only on one side: the right-side actuation increased the lateral offset, whereas the left side actuation decreased the lateral offset. Note that, we always applied a positive DC voltage in this experiment, but denoted the case of decreasing offset (controlled by choosing which set of comb drive to actuate) between two metasurfaces by negative voltage and displacement notations. Hence, with a negative voltage, we observe a longer focal length. Similarly, positive voltage and displacement correspond to an increasing lateral offset and a shorter focal length. An IR camera was aligned with the Alvarez lens and the source to monitor the focal tuning behavior. The distance between the Alvarez metalens and the IR camera was controlled by a motorized linear translation stage to scan across the intensity profiles along the optical axis in microscale fine steps and locate the focal plane tuned by the input voltage. Detailed information on the setup is included in the Supporting Information.

Figure 4a is a camera screenshot showing the two Alvarez metasurfaces overlaying on top of each other. The bottom metasurface sits on a stationary surface while the top metasurface is carried by a MEMS actuator. The comb drives employed to electrostatically displace the top metasurface laterally in opposite directions are partially captured at the edges of the image. By adjusting the distance between the IR camera and the Alvarez lens, a bright focused spot as shown in Figure 4b was found approximately  $200\ \mu\text{m}$  away from the Alvarez lens. We attribute this discrepancy between theory and experimental results on the focal tuning range of the Alvarez lens to the small aperture and the  $50\ \mu\text{m}$  axial separation between the metasurfaces. To test the effect of the aperture size, we measured the focus tuning of several Alvarez lenses without MEMS actuation with various aperture sizes. In these lenses, the lateral separation was actuated manually, and we found a higher tolerance to misalignment and hence a better match between the theory and the experiment as the aperture size increased (see Figure S4 in the Supporting Information). In the experiment of

the MEMS-actuated Alvarez metalens, at every applied voltage, the intensity profile along the optical axis was captured over a 100  $\mu\text{m}$  range around the brightest spot with an increment of 1  $\mu\text{m}$ . We processed the captured data to reduce image noise. Baseline references at no illumination and full illumination were taken to remove anomalies due to camera artifacts by comparison and subtraction. Gaussian filters were then applied to smooth out the random noise while minimizing the blurring of the high-intensity region.

With the aid of the camera screenshots capturing the actuator as shown in Figure 4a, the actuated displacement at an applied voltage was determined from the change in the lateral position of the actuated platform relative to its neutral position using edge detection. Figure 4e and 4f plot the actuated displacement of the top metasurface at various applied voltages, and as shown by Eq. (3), the displacement electrostatically actuated with the comb drives is quadratically dependent on the actuation voltage and hence can be well controlled for any calibrated system. The total stiffness of the folded flexures in the Alvarez system can be calculated from the quadratic fit from the displacement-voltage plots, giving 0.590 N/m when actuated towards the negative direction and 0.586 N/m towards the positive, verifying the symmetry of the mechanical design. The actual stiffness values are 12% smaller than the predicted values presented earlier, which we ascribe to fabrication discrepancies resulting in reasonable deviations in both electrostatic and restoring forces.

For each set of scanned data with the same actuation voltage, a 1D slice of intensities was taken from each screenshot at the same location across the central bright spot. All the 1D slices were then combined into a 2D intensity plot over the scanning distance along the optical axis, as shown in Figure 4c and 4d. In the combined plots, the intensities were normalized, and a threshold was taken to identify and isolate the region of high intensities. The focal position along the optical

axis was calculated by locating the weighted centroid of the pixels above the defined intensity threshold to minimize the effect of background noise. Such absolute positions of the focal spots are estimations due to the difficulty in the visual determination of the zero plane at the device surface. In order to better visualize the focal tuning behavior, the net change in focal position was instead plotted as a function of actuation voltage in Figure 4e, using the corresponding neutral focal position without voltage application as the reference. Such a focal-voltage relation is then translated to a function of actuated displacement in Figure 4f using the displacement-voltage data pairs presented in Figure 4c and 4d. Figure 4e and 4f show the focal locations identified by the weighted centroids of high-intensity clusters above various threshold choices. A tighter threshold percentile gives rise to a smaller isolated region of high-intensity pixels for focal search – 1% corresponds to a bright area of  $18 \mu\text{m}^2$  while 5% corresponds to a bright area of  $90 \mu\text{m}^2$ . As shown in Figure 4f, the Alvarez metalens has produced a tunable focal length range of  $68 \mu\text{m}$  with a total actuated displacement of  $6.3 \mu\text{m}$ , generating a focal length tuning range that is over 10 times larger than the actuated displacement. With the neutral focal length of  $216 \mu\text{m}$ , this focal tuning range corresponds to 1460 diopters change in optical power. At sub-micron displacement steps realized with electrostatic actuation, transition states have been observed in the focal tuning curves due to axial separation between the metasurfaces from the bonding spacer. With a larger focus spot defined with a lower threshold percentile, a smoother tuning behavior can be produced with a slightly smaller range of tuning due to the asymmetric intensity distribution along the optical axis.

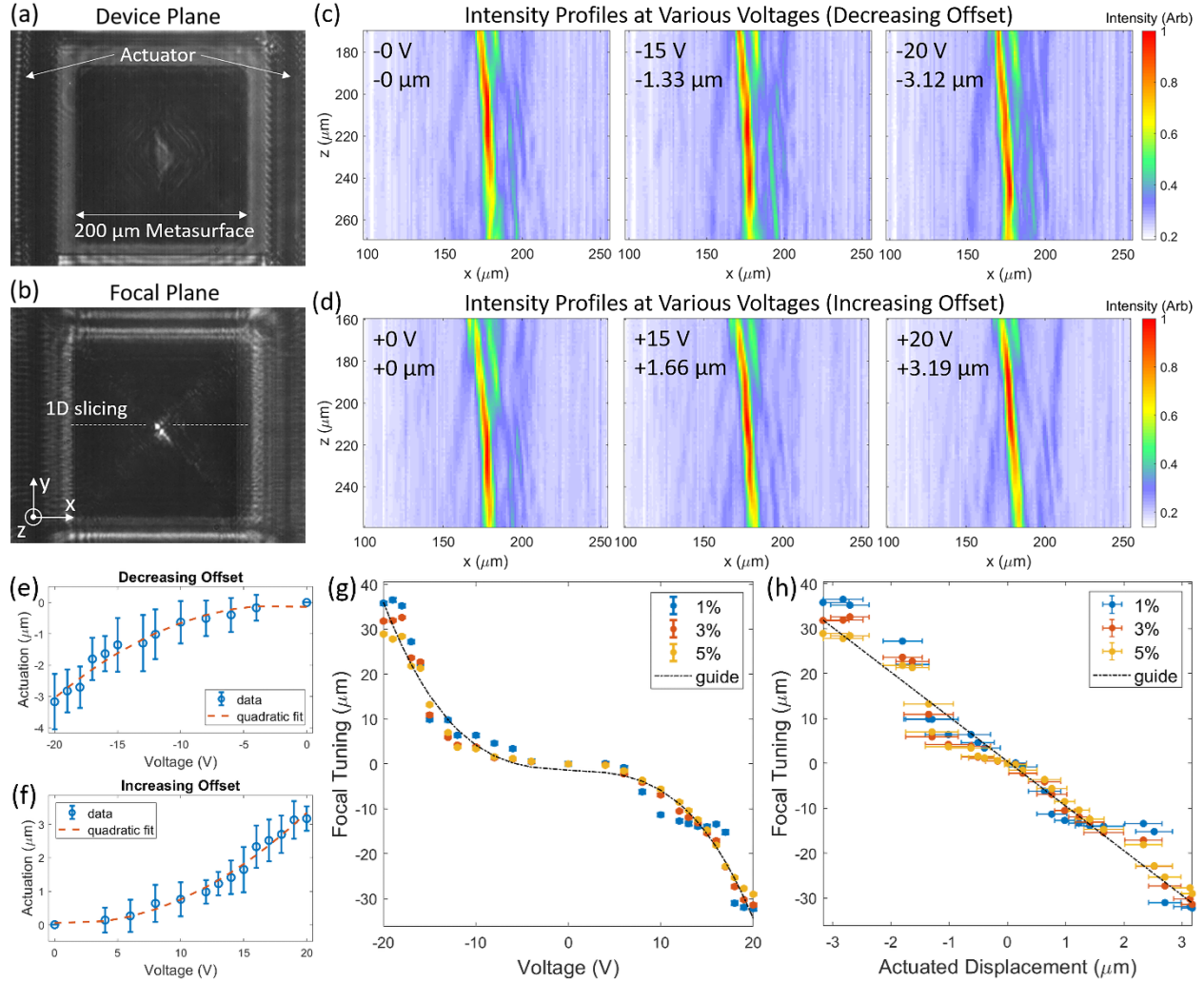


**Figure 4.** IR camera screenshots at (a) the device plane and (b) the focus plane of an Alvarez metalens illuminated with a 1550 nm SLD source. The shift of focal intensity profiles along the optical axis with (c) decreasing and (d) increasing center-to-center offsets between the Alvarez metasurfaces at various actuation voltages and displacements. (e, f) Actuated displacement as a function of applied voltage with negative (positive) actuation corresponds to a decreasing (increasing) offset. (g) Tuning in focal location as a function of applied voltage and (h) as a function of actuated displacement with focus size defined by various intensity thresholds, giving a focal tuning range 10 times larger than the actuated Alvarez displacement. The black dash-dotted lines are provided as guides to the eye.

## Discussion:

Although in the work reported here, we have mainly focused on a MEMS-actuated Alvarez metalens with a 200  $\mu\text{m}$  square aperture, Alvarez metalenses with larger apertures have been

demonstrated with manual actuation [1, 2] and the Alvarez tuning principle is capable of continuously producing further focal tuning with an increasing lateral displacement between the two optical elements while maintaining high tuning efficiency. With the successful demonstration of the current MEMS Alvarez metalens, a larger lateral actuation can be achieved by reconfiguring the electrostatic MEMS actuator design or adjusting the actuation voltage below snap-in. The focusing behavior is significantly affected by the axial separation between the two Alvarez metasurfaces created during bonding. To mitigate this, a thinner spacer layer is desirable and a larger area of Alvarez metasurfaces can be implemented to increase the aperture size.

While this work has demonstrated a MEMS-actuated metasurface Alvarez lens operating in the IR spectrum, others have reported a metasurface-based Alvarez lens operating for visible wavelength when manually displaced on a fine translation stage [1]. While our current Alvarez metasurfaces are fabricated with silicon nitride nanoposts on a silicon membrane or substrate, the silicon underneath the Alvarez metasurfaces can be replaced with silicon oxide or quartz to create a clear optical path for the visible wavelength operation. Such an approach is possible for our choice of comb drive actuation, unlike the parallel plate actuation [14], where the silicon was present in the optical path as the electrodes for vertical displacement.

### **Conclusion:**

We have designed, fabricated, and characterized a MEMS-actuated metasurface lens with a tunable focus modulated based on an Alvarez lens design. With voltage application below 20 V, actuated displacement of 6.3  $\mu\text{m}$  has given rise to a focal length modulated over a range of 68  $\mu\text{m}$ , corresponding to more than 10 times scaling between the actuation input and focal tuning output. The MEMS electrostatic actuation using linear comb drives provides high controllability for its quadratic relation between the actuated displacement and actuation voltage. Replacing bulky

freeform optics with flat, wavelength-scale thick metasurfaces together with the MEMS-driven Alvarez structure will allow the ultimate miniaturization of optical devices with tunable focal length, making them more mechanically and thermally robust, with advantages such as fast tuning, compact size, simple packaging, and low energy consumption.

Such MEMS-actuated Alvarez metalenses with a tunable focus in IR or visible frequencies will have great potentials in 3D imaging and depth-sensing applications such as realizing mixed reality displays [24-26] and ultra-compact endoscopes [19, 27]. Additionally, by using a pair of quartic metasurfaces and computational imaging, the color information can be incorporated in a similar tunable geometry [28]. Their full compatibility with well-established semiconductor microfabrication technologies allows them to be mass-produced with high reproducibility.

**Acknowledgment:**

This work is supported by the fund provided by TunOptix Inc. Part of this work was conducted at the Washington Nanofabrication Facility (WNF) / Molecular Analysis Facility (MAF), a National Nanotechnology Coordinated Infrastructure (NNCI) site at the University of Washington, which is supported in part by funds from the National Science Foundation (awards NNCI-1542101, 1337840 and 0335765), the National Institutes of Health, the Molecular Engineering & Sciences Institute, the Clean Energy Institute, the Washington Research Foundation, the M. J. Murdock Charitable Trust, Altatech, ClassOne Technology, GCE Market, Google, and SPTS. The experimental setup and supporting data acquisition have been partially assisted by James Whitehead and Luocheng Huang from the Nano Optoelectronic Integrated System Engineering (NOISE) Lab at the University of Washington.

## Supporting Information:

Metasurface design

Device fabrication

Experimental setup

Experimental data error analysis

Alvarez metalens with manual tuning to explore the effect of aperture size

## Reference:

- [1] A. Zhan, S. Colburn, C. M. Dodson, and A. Majumdar, "Metasurface freeform nanophotonics," *Scientific Reports*, vol. 7, no. 1, p. 1673, 2017/05/10 2017, doi: 10.1038/s41598-017-01908-9.
- [2] S. Colburn, A. Zhan, and A. Majumdar, "Varifocal zoom imaging with large area focal length adjustable metalenses," *Optica*, vol. 5, no. 7, pp. 825-831, 2018/07/20 2018, doi: 10.1364/OPTICA.5.000825.
- [3] S. W. Seo *et al.*, "Microelectromechanical-system-based variable-focus liquid lens for capsule endoscopes," *Japanese Journal of Applied Physics*, vol. 48, no. 5R, p. 052404, 2009.
- [4] R. D. genannt Daweke, M. Kelp, H. Lehr, O. Mönnich, and P. Osiak, "Electromagnetic direct linear drives for medical endoscopes," in *2014 International Conference on Optimization of Electrical and Electronic Equipment (OPTIM)*, 2014: IEEE, pp. 245-251.
- [5] S. M. Kamali, E. Arbabi, A. Arbabi, and A. Faraon, "A review of dielectric optical metasurfaces for wavefront control," *Nanophotonics*, vol. 7, no. 6, pp. 1041-1068, 2018.
- [6] N. Yu *et al.*, "Light propagation with phase discontinuities: generalized laws of reflection and refraction," *Science*, vol. 334, no. 6054, pp. 333-337, 2011.
- [7] A. V. Kildishev, A. Boltasseva, and V. M. Shalaev, "Planar photonics with metasurfaces," *Science*, vol. 339, no. 6125, p. 1232009, 2013.
- [8] F. Monticone, N. M. Estakhri, and A. Alù, "Full control of nanoscale optical transmission with a composite metascreen," *Physical review letters*, vol. 110, no. 20, p. 203903, 2013.
- [9] N. Yu and F. Capasso, "Flat optics with designer metasurfaces," *Nature Materials*, vol. 13, no. 2, pp. 139-150, 2014.
- [10] S. Jahani and Z. Jacob, "All-dielectric metamaterials," *Nature nanotechnology*, vol. 11, no. 1, p. 23, 2016.
- [11] H.-S. Ee and R. Agarwal, "Tunable metasurface and flat optical zoom lens on a stretchable substrate," *Nano Letters*, vol. 16, no. 4, pp. 2818-2823, 2016.
- [12] A. She, S. Zhang, S. Shian, D. R. Clarke, and F. J. S. A. Capasso, "Adaptive metalenses with simultaneous electrical control of focal length, astigmatism, and shift," vol. 4, no. 2, p. eaap9957, 2018.

- [13] T. Roy, S. Zhang, I. W. Jung, M. Troccoli, F. Capasso, and D. Lopez, "Dynamic metasurface lens based on MEMS technology," *APL Photonics*, vol. 3, no. 2, p. 021302, 2018.
- [14] E. Arbabi, A. Arbabi, S. M. Kamali, Y. Horie, M. Faraji-Dana, and A. J. N. c. Faraon, "MEMS-tunable dielectric metasurface lens," vol. 9, no. 1, p. 812, 2018.
- [15] L. W. Alvarez, "Two-element variable-power spherical lens," ed: Google Patents, 1967.
- [16] A. W. Lohmann, "A new class of varifocal lenses," *Applied Optics*, vol. 9, no. 7, pp. 1669-1671, 1970.
- [17] L. W. Alvarez, "Development of variable-focus lenses and a new refractor," *Journal of the American Optometric Association*, vol. 49, no. 1, pp. 24-29, 1978.
- [18] G. Zhou, H. Yu, and F. S. Chau, "Microelectromechanically-driven miniature adaptive Alvarez lens," vol. 21, no. 1, pp. 1226-1233, 2013.
- [19] Y. Zou, W. Zhang, F. S. Chau, and G. Zhou, "Miniature adjustable-focus endoscope with a solid electrically tunable lens," vol. 23, no. 16, pp. 20582-20592, 2015.
- [20] W. Tang, "Electrostatic comb drive for resonant sensor and actuator application," *Berkeley, CA, USA*, 1990.
- [21] D. M. Brouwer, A. Otten, J. Engelen, B. Krijnen, and H. Soemers, "Long-range elastic guidance mechanisms for electrostatic comb-drive actuators," in *International Conference of the European Society for Precision Engineering and Nanotechnology (EUSPEN)*, May, 2010, pp. 41-50.
- [22] L. Zhang, R. Barrett, P. Cloetens, C. Detlefs, and M. Sanchez del Rio, "Anisotropic elasticity of silicon and its application to the modelling of X-ray optics," *Journal of synchrotron radiation*, vol. 21, no. 3, pp. 507-517, 2014.
- [23] A. Zhan, S. Colburn, R. Trivedi, T. K. Fryett, C. M. Dodson, and A. Majumdar, "Low-contrast dielectric metasurface optics," *ACS Photonics*, vol. 3, no. 2, pp. 209-214, 2016.
- [24] C. Hong, S. Colburn, and A. Majumdar, "Flat metaform near-eye visor," *Applied Optics*, vol. 56, no. 31, pp. 8822-8827, 2017.
- [25] D. Lin *et al.*, "Optical metasurfaces for high angle steering at visible wavelengths," *Scientific reports*, vol. 7, no. 1, p. 2286, 2017.
- [26] E. Bayati, S. Colburn, and A. Majumdar, "Metasurface Optics for Ultra-Compact Augmented Reality (AR) Visors," in *CLEO: QELS Fundamental Science, 2019: Optical Society of America*, p. FTh3M. 4.
- [27] S. S. Rege, T. S. Tkaczyk, and M. R. Descour, "Application of the Alvarez-Humphrey concept to the design of a miniaturized scanning microscope," *Optics Express*, vol. 12, no. 12, pp. 2574-2588, 2004.
- [28] S. Colburn and A. Majumdar, "Simultaneous Achromatic and Varifocal Imaging with Quartic Metasurfaces in the Visible," *ACS Photonics*, 2019.